Available online at www.sciencedirect.com
SCIENCE DIRECT
Journal of Nuclear Materials 351 (2006) 303–315
journal of nuclear materials
www.elsevier.com/locate/jnucmat

Deformation mode map of irradiated 316 stainless steel in true stress–dose space

T.S. Byun *, N. Hashimoto, K. Farrell

Oak Ridge National Laboratory, Metals and Ceramics Division, P.O. Box 2008, MS-6151, Oak Ridge, TN 37831, United States

Abstract

Microscopic and macroscopic deformation modes in type 316 stainless steels after low-temperature irradiation have been mapped into the true stress–dose coordinate system. This paper defines and explains the deformation modes in 316 and 316LN stainless steels and suggests the procedures to produce a deformation mode map. A variety of microstructural features such as dislocation tangles and pileups, dislocation channels, stacking faults, and twins have been observed in the deformation of irradiated stainless steels. Attempts were also made to depict macroscopic phenomena such as uniform deformation, necking, and final fracture in the map. Stress criteria for twinning, channeling, plastic instability, and final failure were proposed and used to establish boundaries between the different deformation modes. Two alternative strain localization mechanisms, twinning and channeling, shared the high-dose region. The region of stable plastic deformation became narrower as dose increased, while the elastic deformation region was enlarged with dose and the unstable deformation region was kept unchanged over the whole dose range.
© 2006 Elsevier B.V. All rights reserved.

1. Introduction

It is known that plastic deformation in austenitic stainless steels produces a large variety of microstructures depending on material and testing conditions, which include tangled dislocations, dislocation pileups, stacking faults, twins, dislocation channels, and martensite particles [1–9]. This complex deformation behavior is related to the low-stacking fault energy (SFE) of the austenitic stainless steels (10–20 mJ/m^2) [10–12]. Irradiation hardens 316 stainless steels to a large degree by generating defect clusters and increases a tendency for strain localization by mechanical twinning or dislocation channeling [1,4,8,9]. A method to integrate the microstructural information is mapping the deformation mechanisms in a proper coordinate system. Original deformation mode maps were proposed by Ashby and coworkers [13–15]; where the deformation behavior of a metal were integrated into a diagram to depict the regions of specific deformation modes in terms of stress–temperature coordinates. Recently, the effect of radiation has been considered in the construction of Ashby maps for fcc and bcc metals [16]. Another type of deformation mode map for irradiated materials includes

* Corresponding author. Tel.: +1 865 576 7738; fax: +1 865 574 0641.
E-mail address: byunts@ornl.gov (T.S. Byun).

0022-3115/$ - see front matter © 2006 Elsevier B.V. All rights reserved.
doi:10.1016/j.jnucmat.2006.02.033

those constructed over the engineering strain–dose coordinates. Such deformation mode–dose maps have been constructed for pure nickel and gold [17], and recently for commercial alloys such as A533B steel, 316 stainless steel, and Zircaloy-4 by the authors [1]. The maps in Refs. [1,17] have been produced on the basis of transmission electron microscopy (TEM) results.

The formation of stacking faults and twins in 316 stainless steels has been explained by the responses of partial dislocations to the applied stress; both the empirical results and theoretical analyses confirmed that the true stress (or equivalent stress) was the major parameter that controlled the microscopic deformation modes [8,9]. Further, plastic instability analysis on uniaxial tensile data showed that the tensile plastic instability stress was independent of irradiation dose or of the type of small defect clusters introduced for hardening [18–20]. Although the tensile deformation after irradiation often comprises only a small amount of uniform deformation and a large fraction of necking deformation, this could not be emphasized in the mapping on the engineering strain versus dose coordinates [1]. It is believed, therefore, that the best way to express the effects of radiation on deformation modes is mapping the modes into a true stress versus dose coordinate system.

The objective of the present work is to map the micro and macroscopic deformation modes of the 316 stainless steels into the true stress versus dose space for room temperature deformation. To establish the boundaries between deformation mechanisms and modes, the semi-empirical and theoretical stress criteria for yielding, twinning, dislocation channeling, plastic instability, and fracture were developed and applied. TEM results for the deformation microstructures after low-temperature neutron or ion irradiation were overlaid onto the same map for confirmation.

2. Microscopic deformation modes in 316 stainless steels

Figs. 1–5 represent the microstructures associated with deformation mechanisms of 316 stainless steels. The microstructures in those figures were produced from two variants: a conventional 316 stainless steel (Fe–13.45Ni–17.15Cr–2.34Mo–1.86Mn–0.57Si) and a 316LN stainless steel (Fe–10.2Ni–16.3Cr–2.01Mo–1.75Mn–0.39Si–0.11N). To produce deformation microstructures, miniature tensile specimens were neutron-irradiated at the coolant temperature (60–100 °C) in the high flux isotope reactor (HFIR) at Oak Ridge National Laboratory and deformed by uniaxial loading. Also, 3 mm-diameter TEM disks of 316LN stainless steel were irradiated by 360 keV helium ions at 200 °C in the triple ion beam facility at Oak Ridge National Laboratory and deformed by bend loading. Experimental conditions and mechanical properties are described in detail elsewhere [1,5–9,19,20].

Austenitic stainless steels experience all of the major plastic deformation mechanisms, such as normal dislocation glide, twinning, and channeling, depending on material and testing conditions [1–9].

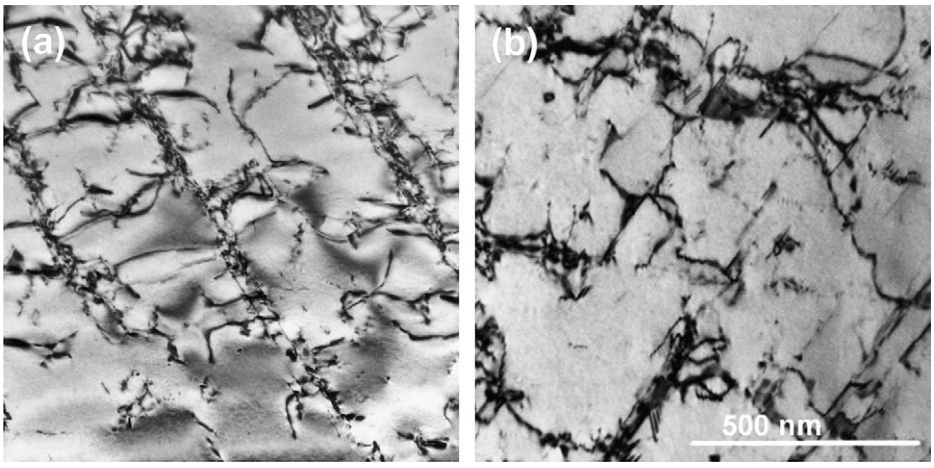

Fig. 1. Dislocation tangles in unirradiated materials: (a) 316 stainless steel tensile-deformed to 16% and (b) 316LN stainless steel bend-deformed to 10%.

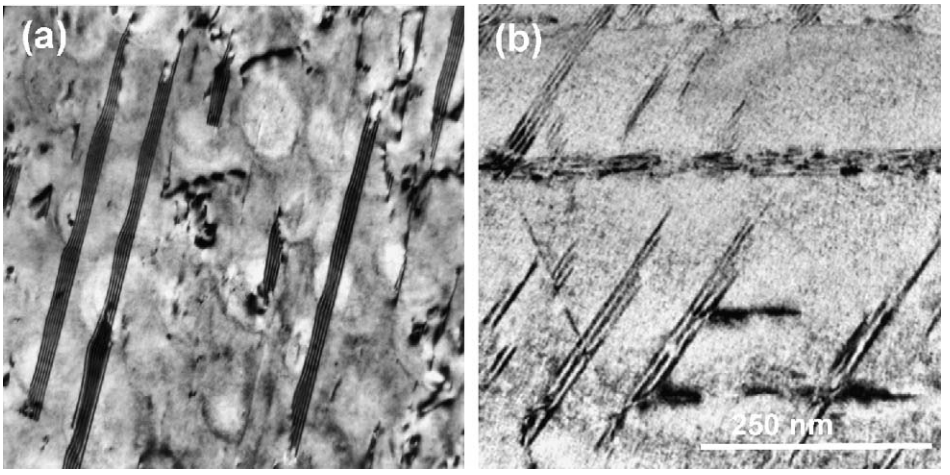

Fig. 2. Stacking faults in 316LN stainless steels: (a) before irradiation, tensile-deformed to 20% and (b) after irradiation to 0.15 dpa by He ions, bend-deformed to 10%.

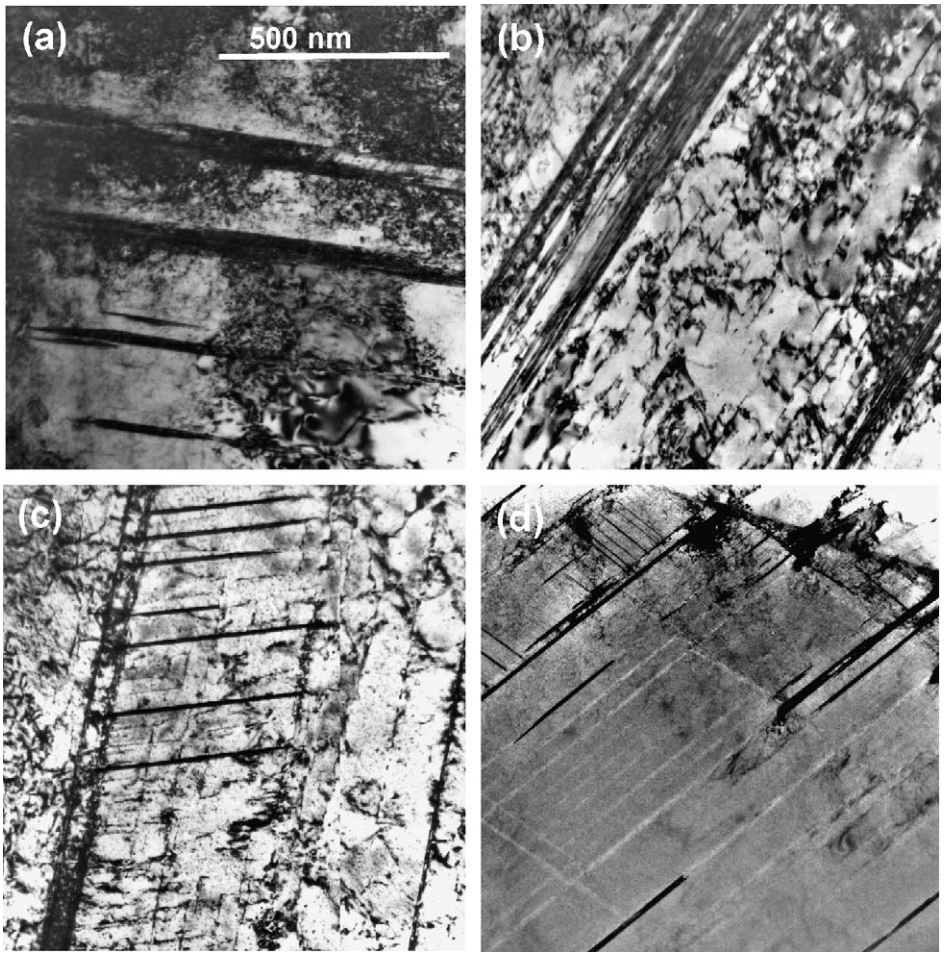

Fig. 3. Twins (dark bands) formed with other features in 316 stainless steel: Twins formed on heavy dislocation tangles (a) at 0 dpa, 57% strain and (b) at 0.001 dpa, 55% strain; twins and tangles (c) and twins (dark bands) and channels (white bands) (d) at 0.15 dpa, 6% strain. Both high-strain and irradiation can result in twins.

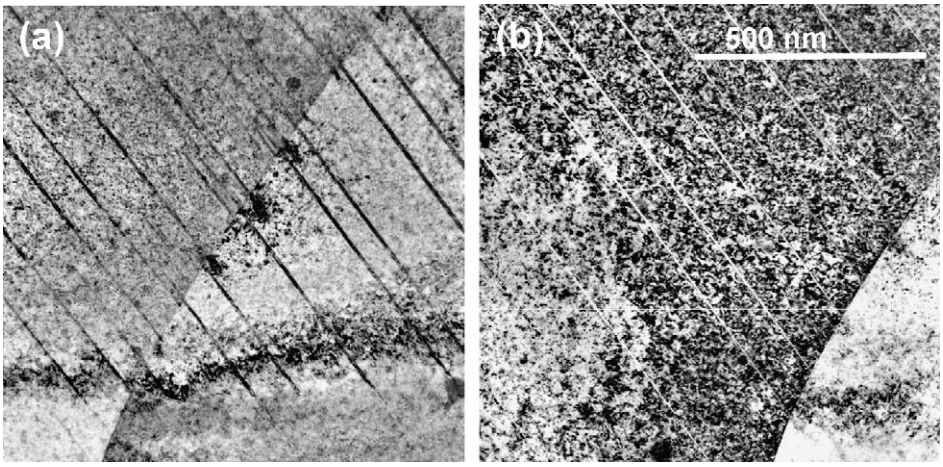

Fig. 4. Twins formed in 316LN stainless steel after He-irradiation to a high-dose of 15 dpa and bend deformation to 10%. Twins propagate through a grain boundary in (a) and an edge-on view of the same area shows white twin lines in (b).

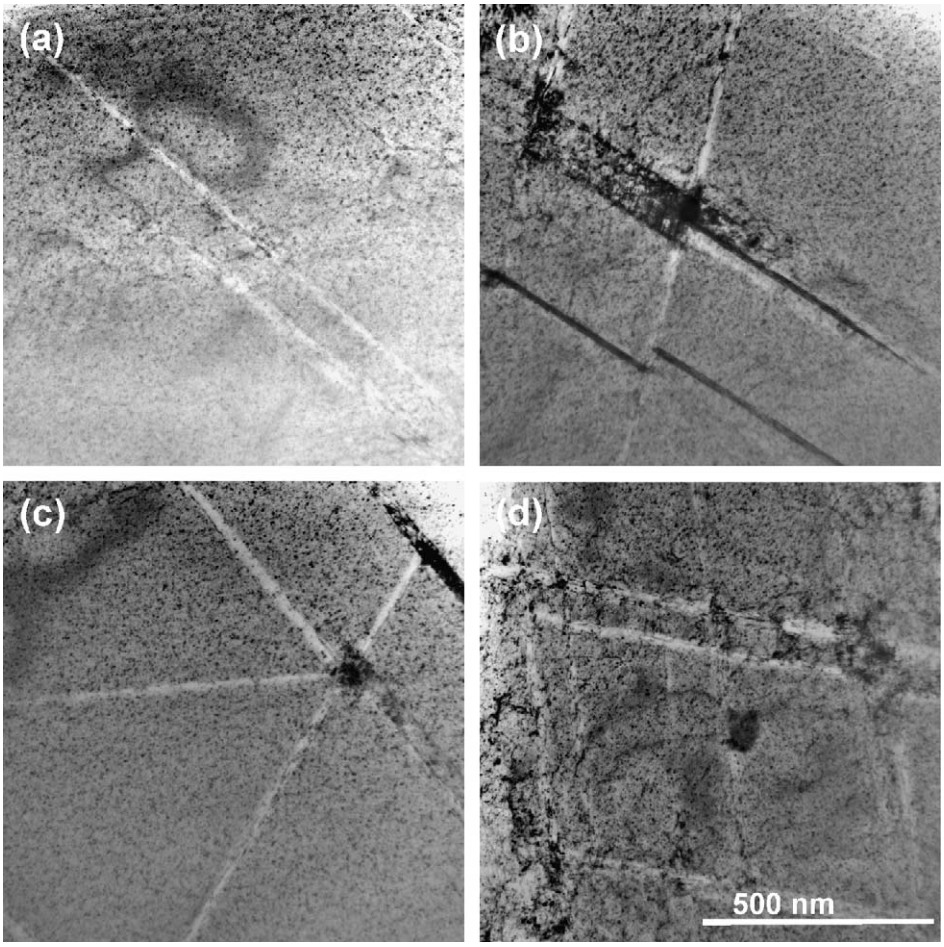

Fig. 5. Channeled microstructures in 316 stainless steel after neutron irradiation to 0.78 dpa at (a) 2%, (b), (c) 5%, and (d) 32% strains. Dark stacking fault or twin fringes are seen in the channels in (b), and a dark fringed band at the upper right corner in (c). The dark region in (c) where three channels intersect is believed to be a dislocation tangle.

The later two mechanisms can be classified as microscopic strain localization [1,8,16]. Although all of those mechanisms are plastic processes involving either ordinary or dissociated dislocations, their microstructural features are obviously differentiated from one another. In the map, the true stress versus dose space consists of regions for dislocation arrays and tangles, stacking faults, twins, and channels. The stacking faults and twins are often accompanied by dislocation tangles and pileups due to local stress fluctuations [9].

Among the deformation microstructures, tangles and pileups of ordinary dislocations are the low-stress deformation products formed by slip on $\{1\,1\,1\}\langle 1\,1\,0\rangle$ systems [5–7]. Fig. 1(a) and (b) show typical features of tangled dislocations in unirradiated 316 and 316LN stainless steels, respectively. Fig. 1(a) displays a preferred alignment along (1 1 1) slip plane. Dislocations are often in planar arrays and form pileups [5–9]. Although the activity of ordinary dislocations is dominant at low-stresses (<400 MPa [8,9]), small stacking faults are frequently visible after room temperature deformation. As the stress level increases, the arrays thicken and form bands on $\{1\,1\,1\}$ planes and random, tangled dislocations appear in the matrix between the bands [14–17]. At a high-strain, cell structures can develop as the bands intercept each other and other dislocation activity occurs to accommodate the non-homogeneous strain distributions [1,9,18]. These low-stress features were dominant in the microstructure following deformation to a few percent strain after irradiation to low-dose (<0.01 dpa) [9] and in the material deformed at temperatures higher than room temperature at higher doses [9,18].

Before twins become dominant at high-stresses ($\geqslant$600 MPa), there might be a transition region in the microstructure if the material can yield below the critical stress for twinning. An evidence for the gradual change is that the separation distance between partial dislocations, or the size of stacking faults, increases from a size barely visible in TEM (~10 nm) to essentially infinite size, or more practically to the effective grain size (~30 μm), over the stress range 400–600 MPa [8,9]. An expression for the separation distance of partials was previously derived as a function of stress [8] and is given in Section 3. The stacking fault segments were formed by dissociation of perfect dislocations (Burgers vector $= a/2\langle 1\,1\,0\rangle$ type, where a is the lattice parameter) into Shockley partial dislocations ($a/6\langle 1\,1\,2\rangle$ type). After helium irradiation small stacking faults with a length of ~0.5 μm were observed at 0.0015 dpa following deformation: The size often increased to a few micrometer at 0.015 dpa; and finally the stacking fault fringes extended over the whole grain at 0.15 dpa [1,9]. Examples of stacking faults with lengths of ~0.5 μm are presented in Fig. 2. Since a large stress fluctuation can exist over the deforming volume, the large stacking faults are often accompanied by low-stress products such as dislocation tangles.

Twinning becomes dominant in high-stress conditions, such as during deformation following low-temperature irradiation to high-doses (>~0.1 dpa), at cryogenic temperatures below ~100 °C, or at strains of 50% or higher in annealed, unirradiated material [1,9,18]. Twins are clearly seen in heavily deformed specimens with heavy dislocation tangles in the background, as seen in Fig. 3(a)–(c). It is known that a mechanical twin layer is formed by glide of partial dislocations on successive planes [5–10]. This mechanism results in a uniform shear strain of 70.7% in the twinned layer [10]. The calculation method for the twinning stress is summarized in Section 3.

Both twinning and channeling are strain localization mechanisms, which are controlled by the type of defect clusters. Channels have been observed primarily in neutron irradiated specimens, where the material was hardened by removable, nanometer size defect clusters [2,16,21–27]. Recent atomistic simulation results [28–30] suggest that the radiation-induced defects may not be completely removed or absorbed by dislocation glides; shearing into smaller defect clusters or transformation into glissile defect clusters can occur during the defect–dislocation interactions. These sheared or transformed defect clusters should act as obstacles to dislocation glide. In the present discussion on channeling, however, it is assumed that the defect clusters produced by neutron irradiation at low-temperature (<100 °C) are almost completely removed by channeling dislocations, and consequently the radiation hardening effect exists little in the channel after the completion of channeling process. On the other hand, the specimens bombarded with He ions deformed by twinning at doses higher than ~0.1 dpa. Irradiation with energetic helium ions can produce gas bubbles as well as displacement damage. The helium bubbles can be sheared, but can not be removed by dislocations. The sheared bubbles with ledges may be harder obstacles than the original spherical bubbles and they might continue to be effective as barriers to

dislocation glide [31–33]. After low-temperature neutron irradiation, however, the defect clusters observed are removable vacancy and interstitial clusters of nanometer size or smaller [5,34]. Since the removal of defects by earlier dislocation glide enabled easier glide for following dislocations, a highly localized deformation band, or channel, can be formed by successive dislocation glide [21–27]. Usually hundreds to thousands of dislocations are involved in the formation of a cleared channel [21–24].

Although the channeling and twinning mechanisms are favored in different specimens with different defect types, both mechanisms can appear in the same specimen after neutron irradiation to 0.15 dpa or higher [1,9]. For example, although most of the deformation bands shown in Fig. 3(c) and (d) contain twins and stacking faults, part of the microstructure also includes fine channels [1]. Numerous short cross-channels and twins intercept the major channels and twins formed on several different slip systems. The common dose range for the two mechanisms seems to be narrow. The difference in deformation microstructures after irradiations with helium ions and neutrons was exacerbated at higher doses ($>\sim$1 dpa), where the effect of helium bubbles on hardening becomes significant in helium irradiated materials [30]. Fig. 4(a) and (b) show the twins formed in 316LN stainless steels after helium irradiation to a high-dose of 15 dpa. An edge-on view shows white lines due to lack of electron deflection in Fig. 4(b). Slight tilting from the edge-on view reveals that some of the defects remain in the twin bands [5–7]; while the contrast of defect-cleared channels is not changed by such slight tilting.

Channeling is largely favored mechanism in specimens after low-temperature neutron irradiation to a dose of 0.78 dpa, as seen in Fig. 5. The defect cleared channels intercept each other and divide the deformation microstructure into blocks with little dislocation activity inside. Dark fringes within channels indicate that there have been partial dislocation activities. Considerable grain-to-grain and in-grain variations were found in the channel widths and spacings [1]. It is known that the active slip systems for channeling are the same as those in unirradiated materials, and an average of 1–3 dislocations travel on each slip plane in the channel which may contain hundreds of slip planes [1,21,26]. Shear strain is well confined in the channel and is uniformly distributed through the width [21,26]. Further, studies indicate that a channel is formed by glide of hundreds to thousands of dislocations in a very short time period of less than a millisecond [24]. Without the contrast from small defects the channeled area appears as a white, cleared path in the bright field TEM images [21]. After deformation by a uniaxial load, the channels formed in a large grain or single crystal material are mostly straight along the easy glide planes [1,21]. In Fig. 5 the width of dislocation channels are relatively uniform for the extended channels, which exclude the small channels with limited lengths. The average width of the developed channels is about 25 nm. Since the {1 1 1} interplanar distance for stainless steel is 0.2062 nm, these dimensions indicate that the channeling process involved about 120 adjacent {1 1 1} planes. Narrower channels have been formed when their growth was limited [22].

3. Stress criteria for deformation modes

3.1. Stacking fault formation and deformation twinning [8]

A stress-based theory for the separation of partial dislocations was proposed and used to explain deformation mechanisms including the formation of large stacking faults and twins in 316LN stainless steel [8,9]. The theory is summarized here and used to calculate the twinning stress and the stresses for selected stacking fault sizes. (Note that all stress terms defined in this section are true stresses.) Force balance equations for the leading and trailing partials with parallel line vectors were established by considering the Peach–Koehler force by applied stress field, the repulsive force between parallel dislocations, the attractive force due to the stacking fault, and the friction force. These components are expressed by the four terms in Eqs. (1) and (2). In these equations, the forward forces or the forces in the applied shear stress direction are defined to have a positive sign and the backward forces to have a negative sign, and all components are defined by force per unit length of dislocation segment [8]:

$$\left[\hat{l}\times\left(\overleftrightarrow{\tau}\cdot\vec{b}_1\right)\right]\cdot\hat{x}-\gamma_{SF}+\frac{G}{2\pi d}\left[\left(\vec{b}_1\cdot\hat{l}\right)\left(\vec{b}_2\cdot\hat{l}\right)+\frac{1}{1-\nu}\left(\vec{b}_1\times\hat{l}\right)\cdot\left(\vec{b}_2\times\hat{l}\right)\right]-f_0=0 \quad \text{for leading partial,} \tag{1}$$

$$\left[\hat{l}\times\left(\overleftrightarrow{\tau}\cdot\vec{b}_2\right)\right]\cdot\hat{x}+\gamma_{\mathrm{SF}}-\frac{G}{2\pi d}\left[\left(\vec{b}_1\cdot\hat{l}\right)\left(\vec{b}_2\cdot\hat{l}\right)+\frac{1}{1-\nu}\left(\vec{b}_1\times\hat{l}\right)\cdot\left(\vec{b}_2\times\hat{l}\right)\right]-f_0=0 \quad \text{for trailing partial,} \tag{2}$$

where $\overleftrightarrow{\tau}$ = stress tensor, $\vec{b}_1$, $\vec{b}_2$ = Burger's vectors for leading and trailing partials, respectively, $\hat{l}$ = line vector (unit vector) of dislocations, $\hat{x}$ = unit vector for x-direction, G = shear modulus, d = separation distance between leading and trailing partial dislocations, ν = Poisson's ratio, f_0 = resistance force to partial dislocation movement in the x-direction. For simplicity, it is assumed that the largest stacking faults are formed by partial glide in the x-direction on the xy-plane with dislocation line vectors in the y-direction. The largest or near-largest shear stress component will be τ_{zx}. Then, the above force balance equations are converted to scalar forms using an angular relationship between partial dislocations, $\theta_2-\theta_1=60^\circ$, where θ_1 and θ_2 are the angles of the Burger's vectors of the leading and trailing partials with the dislocation line vector of the perfect dislocation $\hat{l}$, respectively. Also, defining

$$b_{\mathrm{p}}=|\vec{b}_1|=|\vec{b}_2| \text{ and} \tag{3}$$

$$f(\theta_1,\theta_2)=\cos\theta_1\cos\theta_2+\frac{\sin\theta_1\sin\theta_2}{1-\nu}, \tag{4}$$

the expression for separation distance (d) of partial dislocations was derived by subtracting one force balance equation from the other and by rearranging:

$$d=\frac{Gb_{\mathrm{p}}^2 f(\theta_1,\theta_2)}{\pi(2\gamma_{\mathrm{SF}}-\tau_{zx}b_{\mathrm{p}}|\sin\theta_2-\sin\theta_1|)}. \tag{5}$$

This equation is a generalized expression for the stacking fault size as a function of stress [8]. It indicates that the separation distance increases with resolved shear stress, and the dissociation of a dislocation can increase up to infinity when the resolved stress exceeds a critical value, which becomes the twinning stress as given by Eq. (6). If large stacking faults are visible on a specific {1 1 1} plane, the dissociated dislocations on the plane might be aligned properly for the maximum stress effect. The influence of external stress τ_{zx} is maximized when the Burgers vector of the perfect dislocation $\vec{b}$ coincides with the its line vector $\hat{l}(=\hat{y})$, or the perfect dislocation is of pure screw type ($\hat{l}\parallel\vec{b}\perp\tau_{zx}\hat{x}$), which gives simple angular relationships of the partials with the perfect dislocation: $\theta_1=-30^\circ$ and $\theta_2=30^\circ$.

Glide of the first Shockley partial dislocation leaves an intrinsic stacking fault behind it and needs extra stress to overcome the attractive force due to SFE [10]. It is known that the energies for intrinsic and extrinsic stacking faults and for two twin-matrix interfaces are similar [35]. Therefore, once the intrinsic stacking fault is formed by the glide of the first partial, the glide of a second partial on the next plane forms an extrinsic stacking fault behind it and erases the intrinsic stacking fault. Subsequent glide on the third and successive planes do not need additional stress to overcome the fault energy and form a twin layer [35,36]. Therefore, once the first partial glides, a twin layer can be formed under a high-stress. In the theory discussed in Ref. [8], the twinning stress in polycrystalline material was defined by the critical stress for infinite separation of partials (with Taylor factor = 3.07 [10]):

$$\sigma_{\mathrm{T}}=3.07\tau_{\mathrm{crit}}(d\to\infty)=6.14\frac{\gamma_{\mathrm{SF}}}{b_{\mathrm{p}}}. \tag{6}$$

3.2. Dislocation channeling

The dislocation channeling process has been believed to consist of initial dislocation multiplication, softening due to the removal of defects, strain hardening primarily due to the long range back stress from dislocation pileup at an obstacle such as grain boundary, and propagation through the obstacle [22,24]. Although the channeling phenomenon has been observed in many materials to establish its general features as described in the previous section [21–27] and some mechanisms for dislocation-defect interactions or defect clearing processes have been observed and proposed [37–41,30,42], the criterion for the phenomenon is not clearly determined. A model based on lattice hardening and dislocation pileup was proposed by Makin and Sharp [24] to explain the channel formation in irradiated copper single crystals, in which the critical stress to form a channel is the stress to generate the first dislocation loop in the environment of the defect clusters. In Makin and Sharp's model, however, the role of grain boundaries was not explored. It is believed that the yielding process in irradiated materials is similar to the localized, heterogeneous deformation that occurs during the formation of Lüders bands in hardened materials [1,43]. To explain channeling in the polycrystalline materials, therefore, an integrated

process of dislocation pileup against the grain boundary and subsequent propagation to adjoining grains should be considered. The yield stress is reached when the pileup dislocations can unlock a source in the next grain or propagation occurs into a sufficient volume of the material [43]. A critical stress or corresponding dose level for the channeling is needed to determine the boundary for the channel region. In this study a simple method is proposed to estimate the critical stress for channel propagation. Details such as dislocation generation and interaction with defects were not treated in the method; instead, some microstructural data are used to calculate the critical stress.

When a number of dislocations have accumulated in the pileup against a grain boundary due to clearing of matrix defects, it is unlikely for the pileup dislocations to penetrate the grain boundary one by one. Once a critical stress is reached at the tip of pileup, the pileup dislocations may avalanche into the next grain in the form of two-dimensional pileup or an array. Thus far, it has not been possible to record the channel growth because it is a dynamic process occurring in a short time interval [24]. In order to produce such a rapid dynamic process, the driving force for channel expansion should be a self-sustaining. The stress relaxation due to an abrupt localized shear can be converted to an elastic energy release in a local volume, which is used for the propagation of a dislocation pileup. It is assumed that the radiation-induced defects are completely removed within channels and thus the amount of the stress relaxation is equal to the total hardening stress due to the defects. Since the shear displacement in a channel formed by glide of N_c dislocations of Burgers vector b is $N_c b$, the average shear strain in the channeled area γ_c can be given by

$$\gamma_c = \frac{N_c b}{H_c}, \tag{7}$$

where H_c is a characteristic height, or the range of stress relaxation, in which the hardening stress is relaxed. This characteristic height may decrease as obstacles to dislocation glide increase. Assuming the shear strain within a channel remains constant, finer channels will be formed in the microstructure with more second particles, smaller grains, or more deformation products. (Note that the assumptions made in this model may be for well-developed, ideal channels containing no defects. In reality, the stress change in channeling process should be subjected to a number of complexities such as irregular grain shape, incomplete removal of defects, curved channels, and non-uniform stress distributions.) In the present calculation the effective grain size is used for the height. Then the shear stress relaxed by glide of N_c dislocations is given by

$$\tau_h = G\gamma_c = \frac{GN_c b}{H_c}. \tag{8}$$

Since the stress can not be relaxed below the yield shear stress of defect-free microstructureτ_0, the stress for channeling is given by

$$\tau_C = \tau_0 + \frac{GN_c b}{H_c}. \tag{9}$$

3.3. Plastic instability stress

The plastic instability behavior and its relationship with irradiation hardening have been analyzed for polycrystalline metals after irradiation at low-temperatures (<200 °C) [19,20]. In the analysis the plastic instability stress (PIS) was defined by the true stress at the onset of necking, and calculated from the ultimate tensile stress (UTS) data using:

$$\sigma_{PI} = \mathrm{UTS} \times \exp(\varepsilon_u), \tag{10}$$

where the true plastic uniform strain ε_u is calculated from the uniform elongation UE (in %) using the definition of logarithmic strain:

$$\varepsilon_u = \ln(1 + \mathrm{UE}/100). \tag{11}$$

In the stress–strain analyses it was shown that the plastic instability stress is independent of radiation dose [19,20]. Therefore, the engineering tensile curve after irradiation showed necking at yield when the yield stress was above the plastic instability stress of unirradiated material. These observations are believed to be general phenomena for hardened metallic materials. Further, this plastic instability stress criterion for plastic instability also turned out to be valid for cold worked stainless steels [18]. The plastic instability stress was independent of cold work before testing, and the cold-worked specimens failed by prompt necking at yield when the yield stress reached the plastic instability stress of the annealed material. This plastic instability behavior after pre-strain resembled that of irradiated polycrystalline metals [18–20]. The plastic instability stress is used as the boundary between macroscopically uniform and non-uniform deformation regions in the mapping described below.

3.4. Fracture stress

In the present calculation, the tensile fracture stress and strain are predicted by a model based on the analyses of experimental data [18]. The values for average strain-hardening rate during necking (HRN) were empirically evaluated for the annealed 316LN, 20% cold-worked 316LN, annealed 304, and annealed + irradiated 304 stainless steels, and they were compared with their plastic instability stress values [18]. The comparisons revealed that the magnitude and temperature dependence of HRN were approximately the same as those of the plastic instability stress over the test temperature range. It has been confirmed that the strain-hardening rate is positive during necking in both irradiated and unirradiated materials although the engineering stress decreases with elongation [18–20,44–46]. This should be valid as long as there is a diffuse neck, which occurs usually in ductile metals before a final failure by localized shear (banding) or cleavage initiation. The finding that the strain-hardening rate remains nearly unchanged at plastic instability stress during necking leads to the use of linear true stress–true strain curves for necking deformation. Such high, constant HRN values during necking were explained by a balance between two effects: (1) the decreasing load carrying capability due to cross-section area contraction and due to reduction in hardening rate in the equivalent stress–strain response and (2) the increasing constraint effect from increasing stress triaxiality in the neck.

Assuming a constant strain-hardening rate during necking, the true stress–true strain curve during the necking ($\varepsilon_u \leqslant \varepsilon \leqslant \varepsilon_f$) can be expressed by

$$\sigma(\varepsilon) = \sigma_{PI} + \sigma_{PI}(\varepsilon - \varepsilon_u) = \sigma_{PI}(1 + \varepsilon - \varepsilon_u), \quad (12)$$

where ε_u and ε_f are the true uniform and fracture strains, respectively. Since the values for σ_f and σ_{PI} can be calculated from the engineering stresses, fracture strength (FS) and UTS, using Eq. (10) and

$$\sigma_f = FS \times \exp(\varepsilon_f), \quad (13)$$

we can derive a governing equation:

$$\frac{FS}{UTS} = (1 + \varepsilon_f - \varepsilon_u) \times \exp(\varepsilon_u - \varepsilon_f). \quad (14)$$

The solution for ε_f can be obtained by iterative calculations using this equation and engineering tensile data, and then the fracture stress σ_f is calculated using Eq. (13).

4. Deformation mode map

4.1. Construction of deformation mode map

When determining the domains for deformation modes (for temperatures where thermal creep is not important), the lowest stress criterion should be the yield stress (YS) of the material. The YS sets the boundary between elastic and plastic deformation, and it also enables prediction of deformation mechanism after yielding because it is often controlled by stress [43]. It usually shows a strong dependence on dose and thus the possible stress range for plastic deformation becomes smaller as dose increases. In Table 1 the average yield stresses for 316 stainless steel are listed for various doses up to 0.8 dpa, and the resulting YS bound curve is used in the mapping.

Table 1 also includes plastic instability stress data. These were calculated from UTS and ε_u using Eq. (10). As mentioned previously, the plastic instability stress is almost independent of dose. Further, different versions of type 316 stainless steels, 316, 316LN, and EC316LN had very similar values of plastic instability stress, while the other stress

Table 1
Engineering tensile data and true stress–true strain parameters for 316 stainless steel

Dose (dpa)	YS (MPa)	UTS (MPa)	FS (MPa)	UE (%)	TE (%)	ε_u	PIS (MPa)	ε_f	σ_f (MPa)
0.0	234	579	541	55.60	59.75	0.44	910	0.85	1322
0.0001	272	652	601	60.05	63.30	0.47	956	0.94	1408
0.001	335	654	619	52.25	57.00	0.42	996	0.80	1380
0.01	467	692	640	39.43	42.48	0.33	966	0.78	1394
0.1	571	738	654	36.05	40.20	0.31	1000	0.71	1418
0.78	674	784	732	30.70	33.05	0.27	1024	0.68	1450
Average							975		1395

Note: YS—yield strength; UTS—ultimate tensile strength; FS—fracture strength; UE—uniform elongation; TE—total elongation; ε_u—true uniform strain; PIS—plastic instability stress; ε_f—true fracture strain; σ_f—true fracture stress.

parameters such as yield stress and fracture stress are slightly different among the materials. In the mapping, the average value of 975 MPa was used for drawing the boundary between the uniform deformation and the unstable plastic deformation.

The highest stress that the material can sustain is the true fracture stress. The tensile fracture stress data calculated by Eqs. (13) and (14) are also insensitive to irradiation dose, as seen in Table 1. The average value, 1395 MPa, was used to define the upper limit of the deformation map space. As for true strain parameters, it is worth noting that the true necking strain, or difference between the uniform strain and the fracture strain, is almost independent of dose despite the decrease of both the true fracture strain and the true uniform strain with dose. This indicates that the reduction in ductility, and probably in fracture toughness, by irradiation is mostly due to the loss of uniform ductility.

For stacking fault and twin formation, three stress levels are presented in the map shown in Fig. 6. Table 2 includes the necessary parameters for calculations. As indicated in Eq. (5), the stacking fault size, or separation distance of partials, is a function of stress. In the map, about 400 MPa is displayed as a boundary stress between dislocation tangles and visible stacking faults [8,9]. For 316 stainless steels, the equilibrium (zero stress) separation between partials is about 10 nm and the stacking faults formed by separation of partials more than about 20 nm are regarded as visible ones. Two additional representative stress levels, the stresses for 30 nm and 100 nm separations, were calculated and displayed in the map, which were 440 MPa and 550 MPa, respectively (Taylor factor was 3.07 throughout this study). Also, the twinning stress was determined to be about 600 MPa from Eq. (6). Note that this twinning stress has been derived from the microstructural characterization and used in the theory application to calculate a stacking fault energy value of 14.2 mJ/m^2 for 316

Table 2
Constants (typical) used to calculate stress parameters for microscopic deformation mechanisms

Parameter	Description	Value
a	Lattice parameter	0.3571 nm
b_p	Burger's vector size of partial dislocation	0.1458 nm
b	Burger's vector size of ordinary dislocation	0.2526 nm
d_{111}	Interplanar distance between two nearest {111} planes	0.2062 nm
γ_{SF}	Stacking fault energy	14.2 mJ/m^2
G	Shear modulus	81 GPa
E	Young's modulus	208 GPa
ν	Poisson's ratio	0.291
L	Effective grain size	30 μm
τ_0	Yield shear stress	75 MPa [1]

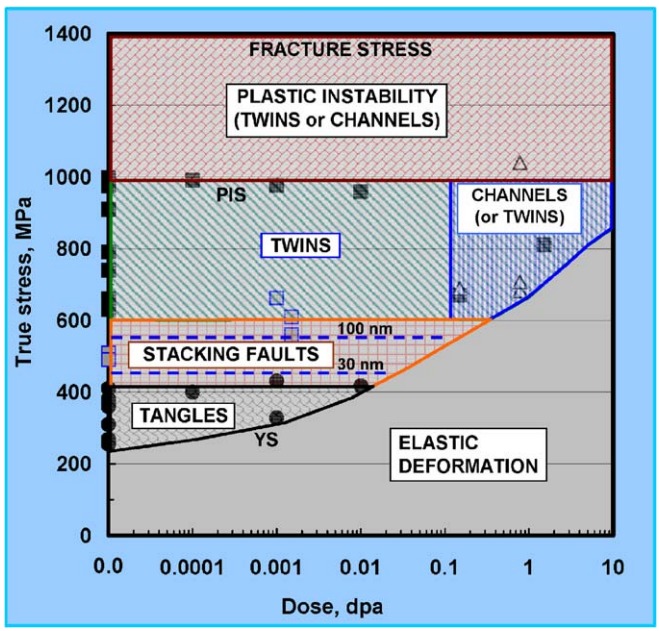

Fig. 6. A deformation mode map for 316 and 316LN stainless steels in the true stress–dose space.

stainless steels, which is reused in the present calculation [8].

Previous mapping by the authors [1] indicated the transition from tangled dislocations to channels was not a gradual procedure occurring over a large dose range. Although the channeling occurring at low-dose and at small strain changed to a dislocation structure as strain increased [17,34], the channeling started to occur at relatively well specified doses; for example ~0.1 dpa in 316 stainless steel, ~0.01 dpa in Zircaloy-4, and ~0.9 dpa in A533B steel [1]. Once channeling occurred, there was not much mixing between tangled dislocations and channels. The dislocations, if observed, were mostly straight [1,21–27]. As described in the previous sections, the channeling process may occur when the following two requirements are satisfied: (1) the stress applied to the region should be higher than a critical stress level, and (2) the defect clusters hardening the material should be removable by dislocations. Plastic deformation will be initiated by formation of channels after irradiation to a critical dose at which yield stress reaches the critical stress for channeling.

Since rapid channel growth was assumed in deriving Eq. (9), the stress determined by this equation must be the critical stress for a well-developed channel only. To use Eq. (9), we need to evaluate the number of channeling dislocations N_c. This was obtained from the channeled microstructures at 0.78 dpa [1]. The largest shifts at channel intersections s_c were about 50 nm (the largest shifts should be used because the projection of the shifts appear smaller when the Burgers vector b is not on the image plane). The size of b is 0.2526 nm for 316 stainless steels. Then the number of dislocations can be calculated by the shift divided by the Burgers vector size; $N_c = s_c/b \approx 200$. Using these values and those in Table 2, Eq. (9) gives 210 MPa for the critical shear stress for channeling (or equivalent stress $\sigma_C = 640$ MPa). This yield stress is achieved in stainless steel irradiated to a dose above 0.1 dpa.

4.2. Discussion on the deformation mode map

Fig. 6 presents the deformation mode map that integrates much of the information described above. Available microstructural data were overlaid in the regions for deformation modes bounded by the stress/dose criteria. The microstructural data confirm that the regions for the different modes are well defined by the stress-based boundary settings. In the previous studies [1], only a few microstructural data were produced for the region of unstable deformation and there was no confirmation on the microscopic mechanisms for the region. This lack of data for necking deformation is partly because the preparation of a good TEM sample is difficult with thin, miniature specimens [1]. Since the plastic instability occurs due to the change of macroscopic geometry, it is believed that the deformation mechanisms are not affected significantly by the onset of necking, but change very gradually, if at all, as the stress and stress constraint in the neck increase with strain. If compared at the same dose levels, therefore, the deformation mechanisms within the plastic instability regime are expected to be similar to those at the onset of plastic instability after uniform deformation.

The deformation mode map shows that the uniform deformation region, which is bounded by yield stress and plastic instability stress, becomes narrower as dose increases, while the elastic deformation region was enlarged with dose by the same amount. The uniform deformation region is predicted to disappear at a dose of ~30 dpa as the yield stress curve crosses the PIS line [19,20]. The region for plastic instability is kept unchanged over the whole dose range. A key improvement found in this new mode map is that the unstable deformation occupies a large fraction of the whole space. This permits the importance of the necking deformation which accounts for at least 50% of total true strain, Table 1, to be presented for its importance. In the previous deformation maps employing an engineering strain versus dose coordinate system, the region for instable deformation was very narrow; most of the necking strains measured were less than 5% in the engineering strain unit [1]. As indicated in Table 1, the necking strain in true strain unit is about 40% over the whole dose range considered.

The most incomplete part in the mapping is drawing a boundary for dislocation channeling. Although short and narrow channels were observed at 0.15 dpa after neutron irradiation, these channels were formed in twinned areas that contained stacking faults and twins [1]. To be regarded as a dominant mechanism, well developed channels should be found over a majority of the deformed area. It is believed that those small channels represent only a local phenomenon and should appear at a mechanism transition from twinning to channeling. Well-developed channels were observed at 0.78 dpa, as seen in Fig 5. Therefore, the critical dose for the

'developed' channels should be in between those two doses. The critical stress determined by Eq. (9) is 640 MPa, which is also between the two yield stresses at those doses, 571 MPa and 674 MPa, respectively. More experimental justification is necessary to obtain an improved critical stress value for channeling.

5. Conclusion

(1) Microscopic and macroscopic room temperature deformation modes and stress parameters in type 316 stainless steels after irradiation have been integrated into a map with true stress–dose coordinates. The true stress–dose space was divided into six different regions representing microscopic and macroscopic features: (1) dislocation tangles (and pileups), (2) dislocation channels, (3) large stacking faults, (4) twins, (5) elastic deformation, and (6) plastic instability and fracture.
(2) To draw boundaries between the regions in the deformation mode map, the stress criteria for twinning, channeling, onset of plastic instability, and final fracture were evaluated using theoretical models and experimental data. Those stress criteria were calculated as 600 MPa, 640 MPa, 975 MPa, and 1395 MPa, respectively.
(3) The microscopic deformation mode at high-doses and high-stresses was dependent on the type of defects. Twinning was favored with non-removable defects such as heavy dislocation tangles and gas bubbles, while dislocation channeling was the alternative mechanism with the removable defect clusters produced by neutron irradiation.
(4) The deformation mode map showed that the region of stable plastic deformation became narrower as dose increased, while the elastic deformation region was enlarged with dose. The region for plastic instability was unchanged over the entire dose range.

Acknowledgements

This research was sponsored by the Offices of Fusion Energy Sciences, US Department of Energy, under Contract DE-AC05-00OR22725 with UT-Battelle, LLC. The authors express special thanks to Drs S.J. Zinkle, Roger E. Stoller, and M.M. Li for their technical reviews and thoughtful comments.

References

[1] K. Farrell, T.S. Byun, N. Hashimoto, J. Nucl. Mater. 335 (2004) 471.
[2] N. Hashimoto, S.J. Zinkle, A.F. Rowcliffe, J.P. Robertson, S. Jitsukawa, J. Nucl. Mater. 283–287 (2000) 528.
[3] H.R. Higgy, F.H. Hammad, J. Nucl. Mater. 55 (1975) 177.
[4] C. Bailat, A. Almazouzi, N. Baluc, R. Schaublin, F. Groschel, M. Victoria, J. Nucl. Mater. 283 (2000) 446.
[5] E.H. Lee, T.S. Byun, J.D. Hunn, M.H. Yoo, K. Farrell, L.K. Mansur, Acta Mater. 49 (2001) 3269.
[6] E.H. Lee, M.H. Yoo, T.S. Byun, J.D. Hunn, K. Farrell, L.K. Mansur, Acta Mater. 49 (2001) 3277.
[7] E.H. Lee, T.S. Byun, J.D. Hunn, K. Farrell, L.K. Mansur, J. Nucl. Mater. 296 (2001) 183.
[8] T.S. Byun, Acta Mater. 51 (2003) 3063.
[9] T.S. Byun, E.H. Lee, J.H. Hunn, J. Nucl. Mater. 321 (2003) 29.
[10] R.W. Hertzberg, Deformation and Fracture Mechanics of Engineering Materials, third ed., John Wiley and Sons, Inc., 1989.
[11] D. Goodchild, W.T. Roberts, D.V. Wilson, Acta Metal. 18 (1970) 1137.
[12] A. Kelly, G.W. Groves, Crystallography and Crystal Defects, J.D. Arrowsmith Ltd., 1970.
[13] M.F. Ashby, Acta Met. 20 (1972) 887.
[14] H.J. Frost, M.F. Ashby, Deformation-Mechanism Maps, Pergamon, 1982.
[15] M.F. Ashby, Materials Selection in Mechanical Design, Pergamon, 1992.
[16] S.J. Zinkle, G.E. Lucas, Fusion Mater. Semiannual Progress Report, DOE-ER-0313/34, September 2003, p. 101.
[17] A. Okada, K. Kanao, T. Yoshiie, S. Kojima, Mater. Trans. JIM 30 (1989) 265.
[18] T.S. Byun, N. Hashimoto, K. Farrell, Acta Mater. 52 (2004) 3889.
[19] T.S. Byun, K. Farrell, Acta Mater. 52 (2004) 1597.
[20] T.S. Byun, K. Farrell, J. Nucl. Mater. 326 (2004) 86.
[21] M.S. Wechsler, The Inhomogeneity of Plastic Deformation, 1971, chapter 2. Am. Soc. for Metals, Metals Park, Ohio.
[22] J.V. Sharp, Acta Met. 22 (1974) 449.
[23] J.V. Sharp, Philos. Mag. 16 (1967) 77.
[24] M.J. Makin, J.V. Sharp, Phys. Status Solidi 9 (1965) 109.
[25] A. Luft, Prog. Mater. Sci. 35 (1991) 97.
[26] R.P. Tucker, M.S. Wechsler, S.M. Ohr, J. Appl. Phys. 40 (1969) 400.
[27] T.H. Blewitt, R.R. Coltman, R.E. Jamison, J.K. Redman, J. Nucl. Mater. 2 (1960) 277.
[28] D. Rodney, Nucl. Instrum. Meth. Phys. Res. Sec. B 228 (2005) 100.
[29] J. Robach, I.M. Robertson, B.D. Wirth, A. Arsenlis, Philos. Mag. 83 (2003) 955.
[30] Y.N. Osetsky, R.E. Stoller, Y. Matsukawa, J. Nucl. Mater. 329–333 (2004) 1228.
[31] E.H. Lee, J.D. Hunn, T.S. Byun, L.K. Mansur, J. Nucl. Mater. 280 (2000) 18.
[32] E.H. Lee, J.D. Hunn, N. Hashimoto, L.K. Mansur, J. Nucl. Mater. 278 (2000) 266.

[33] J.D. Hunn, E.H. Lee, T.S. Byun, L.K. Mansur, J. Nucl. Mater. 282 (2000) 131.
[34] K. Farrell, T.S. Byun, N. Hashimoto, Mapping flow localization processes in deformation of irradiated reactor structural alloys, July 2002, Oak Ridge National Laboratory, ORNL/TM-2002/66.
[35] Z. Jin, T.R. Bieler, Philos. Mag. A 72 (1995) 1201.
[36] Z. Jin, T.R. Bieler, Philos. Mag. A. 71 (1995) 925.
[37] S.M. Bruemer, J.I. Cole, R.D. Carter, G.S. Was, Mater. Res. Soc. Symp. Proc. 439 (1997) 437.
[38] M. Suzuki, A. Sato, T. Mori, Philos. Mag. 65 (1992) 1039.
[39] J.I. Cole, S.M. Bruemmer, J. Nucl. Mater. 225 (1995) 53.
[40] S.G. Song, J.I. Cole, S.M. Bruemmer, Acta Mater. 45 (1997) 501.
[41] Y. Matsukawa, S.J. Zinkle, J. Nucl. Mater. 329–333 (2004) 919.
[42] S.J. Zinkle, Y. Matsukawa, J. Nucl. Mater. 329–333 (2004) 88.
[43] G.E. Dieter, Mechanical Metallurgy, McGraw-Hill, Inc., 1986.
[44] E.V. van Osch, M.I. DeVries, J. Nucl. Mater. 271&272 (1999) 162.
[45] S.M. Ohr, Scripta Metall. 2 (1968) 213.
[46] I.L. Mogfold, D. Hull, J. Iron. Steel Inst. 201 (1963) 55.